Libration points in the Elliptic Restricted Three Body Problem under the combined effects of radiation pressure of primary, oblateness of secondary and Power-law profile of encircling belt

Anindita Chakraborty[1]
Bhilai Institute of Technology, Durg, C. G. India.
acbit10282@gmail.com

(Submitted on 16.05.2022; Accepted on 29.08.2022)

Abstract. The planar elliptic restricted three body problem under the influence of a circumstellar belt is studied in this work. The problem is restricted in the sense that one of the three body is considered to be of so little mass that it does not influence the movement of the other two larger bodies. However, other than the gravitational and other perturbing forces due to the larger primaries, we shall also consider the influence of the force due to the circumstellar or circumplanetary belt. Analytical study of the problem shows existence of four collinear equilibrium points and a pair of triangular equilibrium points of the model. Numerical methods were applied to the Sun-Jupiter system under the influence of the asteroid belt and these show the existence of four collinear and two pairs of non-collinear equilibrium points in the pulsating rotating plane. The numerically obtained results as well as the analytical results were then graphically represented and the influence of the different perturbing forces were studied. The basin of attraction of the equilibrium points for the model is also discussed based on the variation of the perturbing forces.

Key words: Chermynkh-like problem, Elliptic restricted three body problem, power law density profile, fractal basin of attraction

Introduction

The study of restricted three body problem, which found its applicability in a wide range of Space operations such as positioning of satellite, station-keeping, transfer trajectory designing and so on, had started in the form where two large celestial bodies, assumed to be point masses, are revolving in circular orbits and the third body is assumed to be of infinitesimal mass. This representation of few body problem, though not completely solvable, found wide applicability and has since being under study with various generalization and modifications. The foremost modification to the problem was the consideration of the perturbing forces due to luminosity of the body. The oblateness or triaxiality of the body was also found to be an effective perturbation in some cases. Another form of modification of the problem was consideration of the orbits of the primaries to be not circular but elliptical. This version of the problem known as Elliptic Restricted Three Body Problem (ERTBP) was found to be more effective in exploration of long-time dynamics of the model [Szebehely (1967)].

In 1987, Chermynkh [Chermnykh (1987)] presented another modified version of the restricted three body problem by assuming the angular velocity to be greater than one. This increase in the angular velocity can be accounted for considering the perturbation caused by the asteroid belt surrouding the two primaries. Papadakis [Papadakis (2004)] has recently re-invigorated the interest in these types of problems by studying symmetric motions near the three collinear equilibrium points in three-dimensional space under the assumption that the mass parameter is constant while the angular velocity parameter can

vary continuously. He [Papadakis (2005a)] also illustrated the numerical investigations of the equilibrium points and the zero-velocity curves. Papadakis (2005b) also studied asymmetric periodic orbits near triangular equilibrium points when the assumed angular velocity varies for the Sun-Jupiter mass distribution. Further studies were carried out by Jiang and Yeh, who studied a Chermnykh-like problem in which the mass parameter (μ) was set to 0.5, thereby finding both analytically as well as numerically that there are extra equilibrium points. To explain how the belt around the planet affects the system, they used a Chermynkh-like model. Miyamoto-Nagai's profile and Power-Law's profile were used to define the gravitational forces from belts in these studies. Also using the Miyamoto-Nagai profile, Kushvah studied the linear stability of equilibrium points in the generalized photogravitational Chermnykh's problem [Kushvah (2008)], linearized the Hamiltonian in the generalized photogravitational Chermnykh's problem [Kushvah (2009)] and designed trajectory around the Lagrangian point L_2 in the Sun-Earth system [Kushvah (2011)]. Furthermore, he and his co-authors investigated the power-law profile and its impact on the restricted three-body problem under a variety of generalization parameters [Kushvah et al. (2012),Kishor & Kushvah (2013)], etc.

All the above mentioned work is done in the framework of circular restricted three body problem. In the paper [Chakraborty et al. (2021)], the dynamics of the infinitesimal for the planar elliptic restricted three body model interacting with circumstellar belt is studied. In the above paper the potential due to the belt is considered according to finite Mestel ring.

In this paper, the model of elliptic restricted three body problem under the influence of the circumstellar belt is further generalized and improvised by defining the potential due to circumstellar belt by power law profile and adding into consideration the radiation pressure of the largest primary and oblateness of the second primary.

1 Equations of motion

Suppose m_i $(i = 1,\ 2)$ denote the masses of the two primaries M_1 (larger) and M_2 (secondary) and let the mass of the infinitesimal body moving in the plane of the motion of the primaries be m. We suppose that the primaries lie on the x-axis of the inertial plane represented by the coordinates (ξ, η), with the origin at the barycenter of the two primary bodies. The center of the surrounding belt coincides with the barycenter of the primaries. Also, we take into consideration the radiation pressure of the first primary and oblateness of the second primary. If the position of the two primaries in the inertial barycentric frame of reference are (ξ_1, η_1) and (ξ_2, η_2), then equations of motion are given as follows:

$$\ddot{\xi} = -\frac{Gm_1q_1(\xi-\xi_1)}{r_1^3} - \frac{Gm_2(\xi-\xi_1)}{r_2^3}\left(1+\frac{3A_1}{2r_2^2}-\frac{15A_2}{8r_2^4}\right) - \frac{\partial V}{\partial \xi}, \quad (1)$$

$$\ddot{\eta} = -\frac{Gm_1q_1(\eta-\eta_1)}{r_1^3} - \frac{Gm_2(\eta-\eta_1)}{r_2^3}\left(1+\frac{3A_1}{2r_2^2}-\frac{15A_2}{8r_2^4}\right) - \frac{\partial V}{\partial \eta}, \quad (2)$$

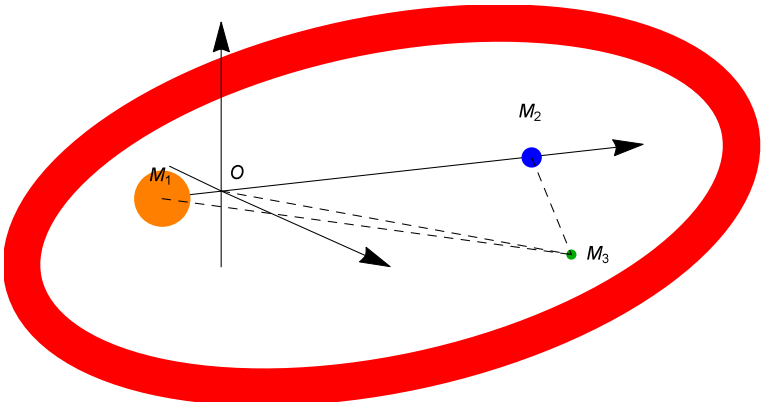

Fig. 1. Geometry of the problem

where,

$$r_1^2 =(\xi-\xi_1)^2+(\eta-\eta_1)^2 \text{ and } r_2^2=(\xi-\xi_2)^2+(\eta-\eta_2)^2. \tag{3}$$

The parameter $q_1 = 1-\beta_1$, where, $\beta_1 = \frac{F_r}{F_g}$, and F_r is the force caused by radiation pressure and F_g is the force due to gravitational attraction, is the radiation factor. The oblateness coefficient of the second primary is denoted by A_i, with $0 < A_i = J_{2i}\mathcal{R}_2^{2i} << 1$, where J_{2i} are zonal harmonic coefficients and $\mathcal{R}_2$ is the mean radii of m_2, assuming that the primaries have their equatorial planes coinciding with the plane of motion. V is denoting the potential due to circumscribing belt.

The body M_2 is orbiting M_1 in an elliptic orbit with eccentricity $'e'$ and semi-major axis $'a'$, then the distance between the primaries is given by

$$\rho =\frac{a(1-e^2)}{1+e\cos f}. \tag{4}$$

Here f is the true anomaly of the first primary.

Taking the angular velocity $\omega = \dot{f}\hat{k}$, where $\dot{f}$ is the rate of change of true anomaly given by

$$\dot{f} =\frac{na^2\sqrt{1-e^2}}{\rho^2}; \tag{5}$$

we transform the coordinate system to rotating coordinate system, using the transformation:

$$\xi =X\cos f - Y\sin f, \tag{6}$$

$$\eta =X\sin f + Y\cos f. \tag{7}$$

Also, we take the sum of masses of the two primaries as unit of mass, distance between the primaries as characteristic length and the period of revolution of the second body as unit of time such that the semi-major axis $a \sim 1$ and gravitational constant $\mathcal{G} \sim 1$. Then, we obtain the following equation of motion in normalized rotating barycentric coordinate system:

$$\begin{aligned}\ddot{X} - 2\dot{Y}\dot{f} - Y\ddot{f} - X\dot{f}^2 =& -\frac{q_1(1-\mu)(X+\mu\rho)}{R_1^3} \\ & -\frac{\mu(X+(\mu-1)\rho)}{R_2^3}\left(1+\frac{3A_1}{2R_2^2}-\frac{15A_2}{8R_2^4}\right)-\frac{\partial V}{\partial X};\end{aligned} \tag{8}$$

$$\begin{aligned}\ddot{Y} + 2\dot{X}\dot{f} + X\ddot{f} - Y\dot{f}^2 =& -\frac{q_1(1-\mu)Y}{R_1^3} \\ & -\frac{\mu Y}{R_2^3}\left(1+\frac{3A_1}{2R_2^2}-\frac{15A_2}{8R_2^4}\right)-\frac{\partial V}{\partial Y}\end{aligned} \tag{9}$$

where,

$$R_1^2 = (X+\mu\rho)^2 + Y^2 \text{ and } R_2^2 = (X+(\mu-1)\rho)^2 + Y^2 \tag{10}$$

Here, $\mu = \frac{m_1}{m_1+m_2}$. V is the potential due to the disc which is given by [Kushvah et al. (2012), Yeh& Jiang (2006)]

$$V = -4\int_{r'} \frac{F(\zeta)\rho'(R')R'}{R+R'}dR', \tag{11}$$

where $F(\zeta)$ denotes the elliptic integral of first kind, R' is the disk's reference radius and $\zeta = \frac{2\sqrt{RR'}}{R+R'}$.

Then the gravitational force of the disc [Yeh& Jiang (2006)]

$$f_b(R) = -\left(\frac{dV}{dR}\right)_{R=R_m} = -2\int \frac{\rho'(R')R'}{R+R'}\left[\frac{E(\zeta)}{R+R'}+\frac{F(\zeta)}{R+R'}\right]dR'; \tag{12}$$

where, $E(\zeta)$ is the elliptic integral of the second kind. The power law density profile of the disc, having thickness $h \approx 10^{-4}$ is $\rho(R) = cR^{-p}$, $p = 3$ and c, is constant determined with help of disc mass. Calculating $f_b(R)$ at $R = R_m = 0.99$ and expanding integrals in equation (11) and (12) with the limit $b \leq R' \leq a$ and choosing appropriate term relative to R, the simplified form of $f_b(R)$ [Jiang & Yeh (2006)] is obtained as

$$f_b(R) = -\frac{2ch\pi}{R^2}\left(\frac{a-b}{ab}\right) - \frac{3ch\pi}{8}\frac{1}{R^3}\log\left(\frac{a}{b}\right)\Bigg|_{R=R_m}. \tag{13}$$

Here, a and b are inner and outer radii of the belt. Further transforming the coordinate system to pulsating coordinate system, using the transformation

$X = \rho\bar{x}$, $Y = \rho\bar{y}$ and employing the equations (12) and (13), we get the system of equations:

$$\begin{aligned}\bar{x}'' - 2\bar{y}' =& \frac{1}{1+e\cos f}\left[\bar{x} - \frac{1}{n^2}\left\{\frac{q_1(1-\mu)(\bar{x}+\mu)}{\bar{r}_1^3}\right.\right.\\ &+ \frac{\mu(\bar{x}+\mu-1)}{\bar{r}_2^3}\left(1 + \frac{3A_1}{2\bar{r}_2^2}(1+e\cos f)^2 - \frac{15A_2}{8\bar{r}_2^4}(1+e\cos f)^4\right)\\ &\left.\left. + \frac{2ch\pi(a-b)}{ab}\frac{\bar{x}}{\bar{r}^3} + \frac{3ch\pi}{8}\log\frac{a}{b}\frac{\bar{x}}{\bar{r}^4}(1+e\cos f)\right\}\right]; \qquad (14)\end{aligned}$$

$$\begin{aligned}\bar{y}'' + 2\bar{x}' =& \frac{1}{1+e\cos f}\left[\bar{y} - \frac{1}{n^2}\left\{\frac{q_1(1-\mu)\bar{y}}{\bar{r}_1^3}\right.\right.\\ &+ \frac{\mu\bar{y}}{\bar{r}_2^3}\left(1 + \frac{3A_1}{2\bar{r}_2^2}(1+e\cos f)^2 - \frac{15A_2}{8\bar{r}_2^4}(1+e\cos f)^4\right)\\ &\left.\left. + \frac{2ch\pi(a-b)}{ab}\frac{\bar{y}}{\bar{r}^3} + \frac{3ch\pi}{8}\log\frac{a}{b}\frac{\bar{y}}{\bar{r}^4}(1+e\cos f)\right\}\right]; \qquad (15)\end{aligned}$$

where,

$$\bar{r}_1^2 = (\bar{x}+\mu)^2 + \bar{y}^2 \text{ and } \bar{r}_2^2 = (\bar{x}+\mu-1)^2 + \bar{y}^2 \qquad (16)$$

2 Mean motion

In the elliptical case, the distance between the primaries is given by (4) so that the mean distance between them is obtained as $\frac{a(1-e^2)}{\sqrt{1+e^2}}$. We have assumed the eccentricity of the orbit of the primary M_1 and the eccentricity of the orbit of the primary M_2 are both equal to e. Then the equation of mean motion [Idrisi et al. (2021)] is simplified as

$$n^2 = 1 + \frac{3}{2}e^2. \qquad (17)$$

Then the pseudo mean motion, including the effect due to radiation pressure of largest primary, oblateness of the second primary and precision effect due to the presence of circumstellar belt, is given by

$$n^2 = q_1 + \frac{3}{2}\left(e^2 + A_1 - \frac{5}{4}A_2\right) - 2f_b(\bar{r})\Big|_{\bar{r}=\bar{r}_m}. \qquad (18)$$

3 Position of equilibrium points

The critical values of the potential function $\Omega(\bar{x}, \bar{y}, \bar{z}, f)$ are determined as the equilibrium points of the system of differential equations (14) and (15). These

equilibrium points are also known as Libration points or Lagrangian points. The position of the five Lagrangian points, with the solar radiation pressure of one of the primaries taken into account(neglecting the effect of drag forces), was analyzed in the case of ERTBP [Ammar (2008)]. However, it has been studied that the Lagrangian equilibrium points in the classical problem (i.e., CRTBP) shift their location when the other perturbation forces are considered. This section is focused on the study of the position of the equilibrium points in ERTBP when the potential due to circumstellar belt is also considered along with radiation pressure of the largest primary and oblateness of the second primary.

At the equilibrium points, the particle has zero velocity and acceleration, therefore taking $\bar{x}'' = \bar{x}' = \bar{y}'' = \bar{y}' = 0$ in equation (14) and (15), we consider the equations

$$n^2\bar{x} - \left\{ \frac{q_1(1-\mu)(\bar{x}+\mu)}{\bar{r}_1^3} + \frac{\mu(\bar{x}+\mu-1)}{\bar{r}_2^3}\left(1 + \frac{3A_1}{2\bar{r}_2^2}\left(1+e\cos f\right)^2 \right.\right.$$
$$\left.\left. - \frac{15A_2}{8\bar{r}_2^4}\left(1+e\cos f\right)^4\right) + B_1\frac{\bar{x}}{\bar{r}^3} + B_2\frac{\bar{x}}{\bar{r}^4}\left(1+e\cos f\right)\right\} = 0; \tag{19}$$

$$n^2\bar{y} - \left\{ \frac{q_1(1-\mu)\bar{y}}{\bar{r}_1^3} + \frac{\mu\bar{y}}{\bar{r}_2^3}\left(1 + \frac{3A_1}{2\bar{r}_2^2}\left(1+e\cos f\right)^2 - \frac{15A_2}{8\bar{r}_2^4}\left(1+e\cos f\right)^4\right)\right.$$
$$\left. + B_1\frac{\bar{y}}{\bar{r}^3} + B_2\frac{\bar{y}}{\bar{r}^4}\left(1+e\cos f\right)\right\} = 0; \tag{20}$$

where,

$$B_1 = \frac{2ch\pi(a-b)}{ab},$$
$$B_2 = \frac{3ch\pi}{8}\log\frac{a}{b}.$$

For numerical explorations, consider the model to be composed of an infinitesimal particle affected by the forces due to the Sun as radiating primary and Jupiter as the oblate second primary. The oblateness factors for the second primary are assumed to be $A_1 = 0.005$ and $A_2 = 0.005$, respectively. The inner and outer radius are assumed to be $b = 1$ and $a = 1.5$ respectively, control factor of density profile $c = 1910.83$ and disk thickness $h = 0.0001$. For analytical and numerical study of the effect of the perturbation due to the circumstellar belt, we are using the notation B_1 and B_2 to denote the two parts of the perturbing force. Figure 2 shows two set of curves depicting the equations (19) and (20) and, hence, the point of intersection of these two curves are the critical points of the system. However, the equilibrium points depicted in these figures are numerically obtained. In this figure, the shift in the position of the equilibrium points, when the perturbing forces such as the radiation pressure of the largest primary, the oblateness of the second primary and the influence

of force due to the circumstellar belt is considered from that of the case when these forces are neglected, is made. It was observed that when the perturbing forces are neglected the model shows the presence of five equilibrium points same as observed in CRTBP (see fig. 2). However, when the perturbing forces are considered, numerical study of the system shows the presence of eight equilibrium points, of which five equilibrium points are analogues to the classically obtained Lagrangian equilibrium points $L_1,\ L_2,\ L_3$ (collinear points), L_4 and L_5(triangular points). Out of the three newly obtained equilibrium points, a pair of non-collinear points are equidistantly placed above and below the $y-$axis and the third is lying on the $x-$axis between the largest primary and collinear equilibrium point L_1.

Figures 3 to 6 present the study of the behavior of the above mentioned model varying the different perturbing forces. Figure 3 depicts the shift in the position of the points when the radiation pressure is reduced from 1 to 0.6. It was observed that the triangular equilibrium points show substantial shift, they are moving farther from x-axis and towards y-axis. Also the equilibrium point $L_3, L_{3\alpha}$ show shift towards the largest primary. To study the effect of the circumstellar belt, the thickness of the belt h is varied from 0 to 0.0003. The curves are drawn in figure 4 corresponding to three values $h = 0, 0.0001, 0.0003$. It was found that for $h = 0$, the equilibrium point $L_3\alpha$ vanishes and the points $L_3, L_4, L_5, L_{4(N)}$ and $L_{5(N)}$ show shift in position with increased value of h. Figures 5 and 6 represent the shift in the position of the equilibrium points with respect to the two factors of oblateness A_1 and A_2 which are varied as 0, 0.05, 0.1. The position and existence of many of the equilibrium points were found to be affected by A_2. A general though slight shift in position of all equilibrium points was observed varying A_1, whereas when A_2 is increased the number of equilibrium points decreased from eight to five and then to one.

3.1 The Triangular equilibrium points

Now to get the coordinates of triangular equilibrium points, we solve the equations (19) and (20), taking $y \neq 0$. From equation (20), we have

$$n^2 - \left\{ \frac{q_1(1-\mu)}{\bar{r}_1^3} + \frac{\mu}{\bar{r}_2^3}\left(1 + \frac{3A_1}{2\bar{r}_2^2}(1+e\cos f)^2 - \frac{15A_2}{8\bar{r}_2^4}(1+e\cos f)^4\right) + B_1\frac{1}{\bar{r}^3} + B_2\frac{1}{\bar{r}^4}(1+e\cos f)\right\} = 0 \tag{21}$$

Then, equation (19) reduces to:

$$\frac{q_1(1-\mu)\mu}{\bar{r}_1^3} + \frac{\mu(\mu-1)}{\bar{r}_2^3}\left(1 + \frac{3A_1}{2\bar{r}_2^2}(1+e\cos f)^2 - \frac{15A_2}{8\bar{r}_2^4}(1+e\cos f)^4\right) = 0 \tag{22}$$

In absence of all perturbing forces other than the radiation pressure of the largest primary, the solution of the system of equations is given by

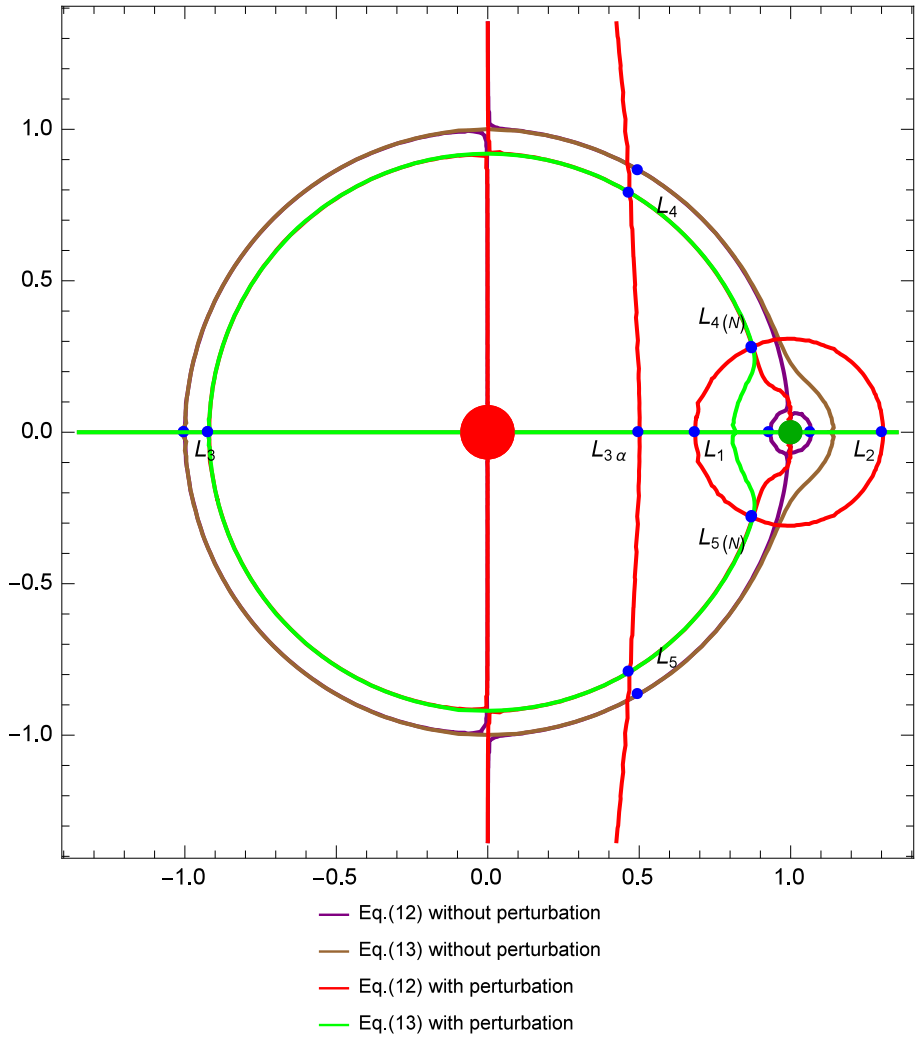

Fig. 2. A comparative representation of equilibrium points in the Sun-Jupiter system with and without the perturbing forces

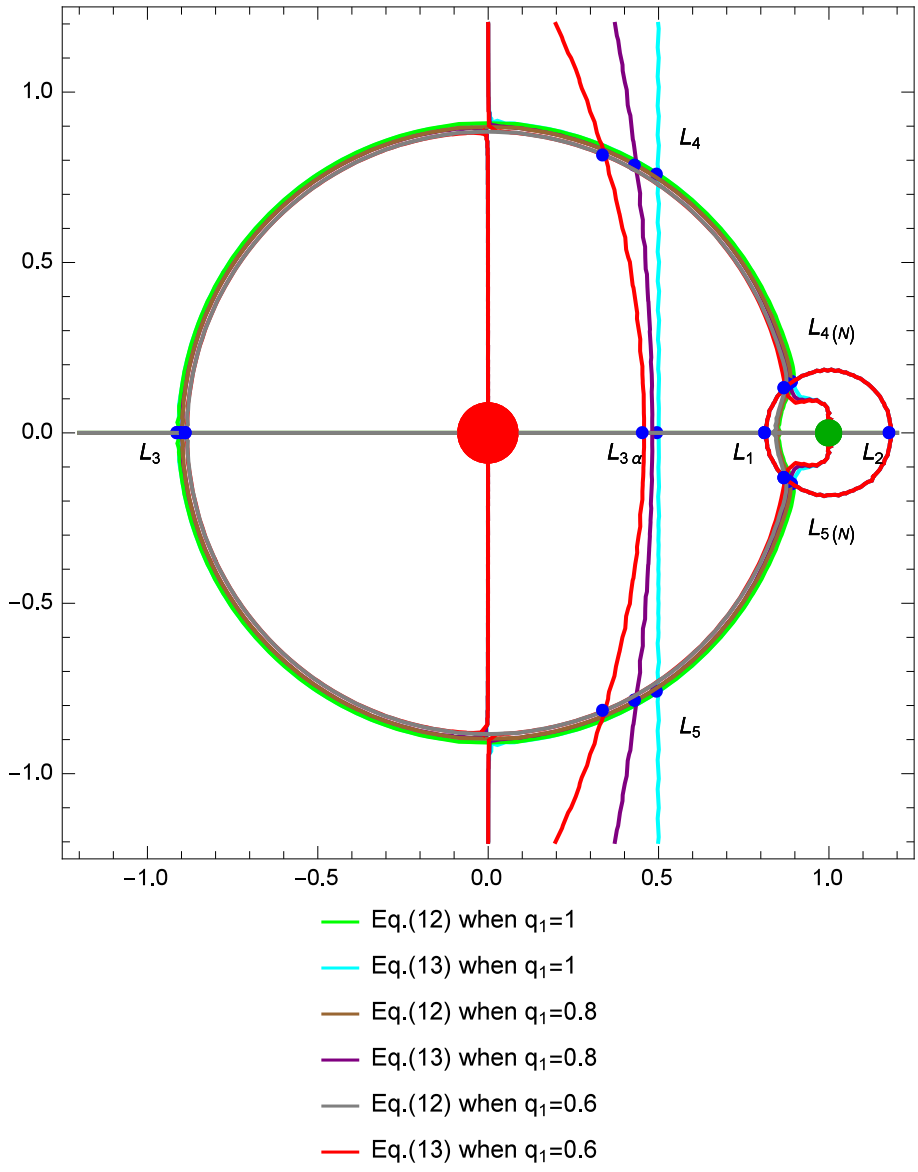

Fig. 3. The shift in the equilibrium points due to the effect of radiation factor q_1 of the massive primary. The blue dots represent the numerically obtained position of the planar equilibrium points.

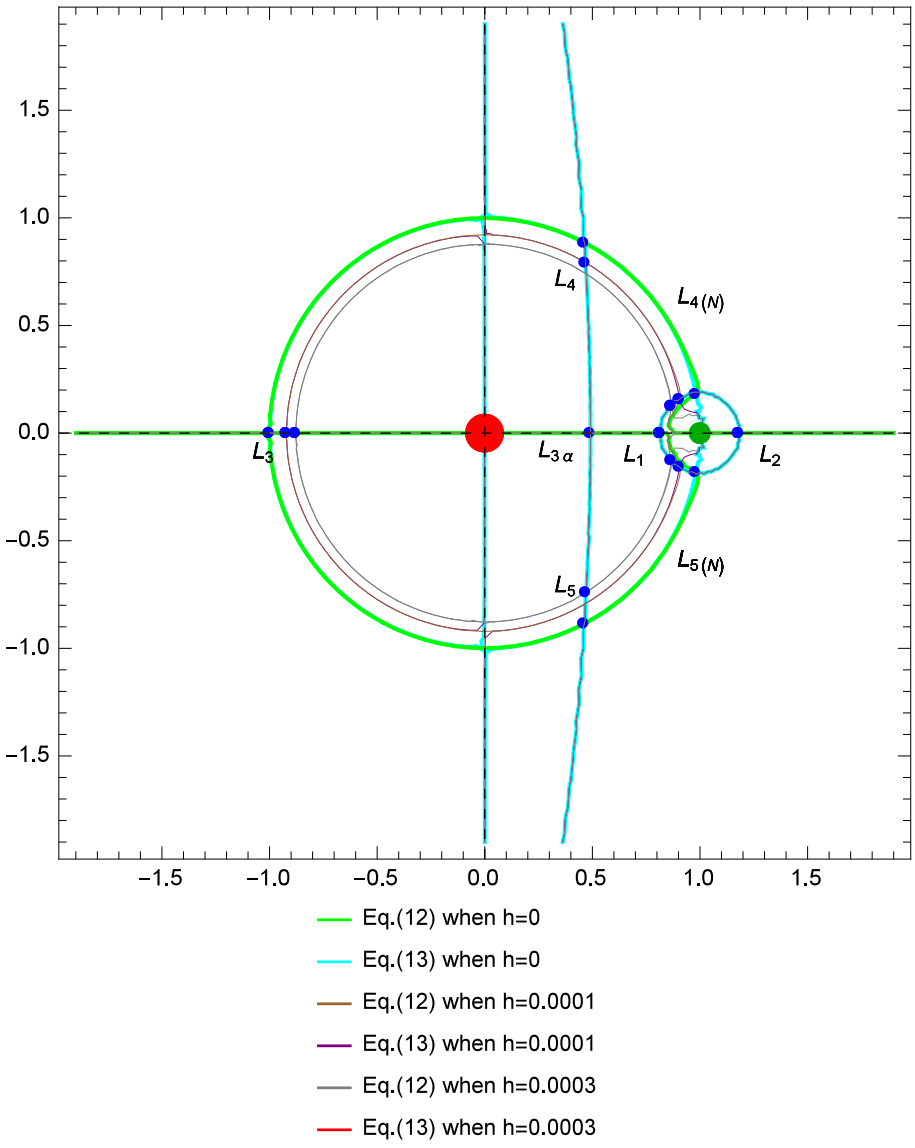

Fig. 4. The shift in the equilibrium points due to the effect of the circumstellar belt. The blue dots represent the numerically obtained position of the planar equilibrium points.

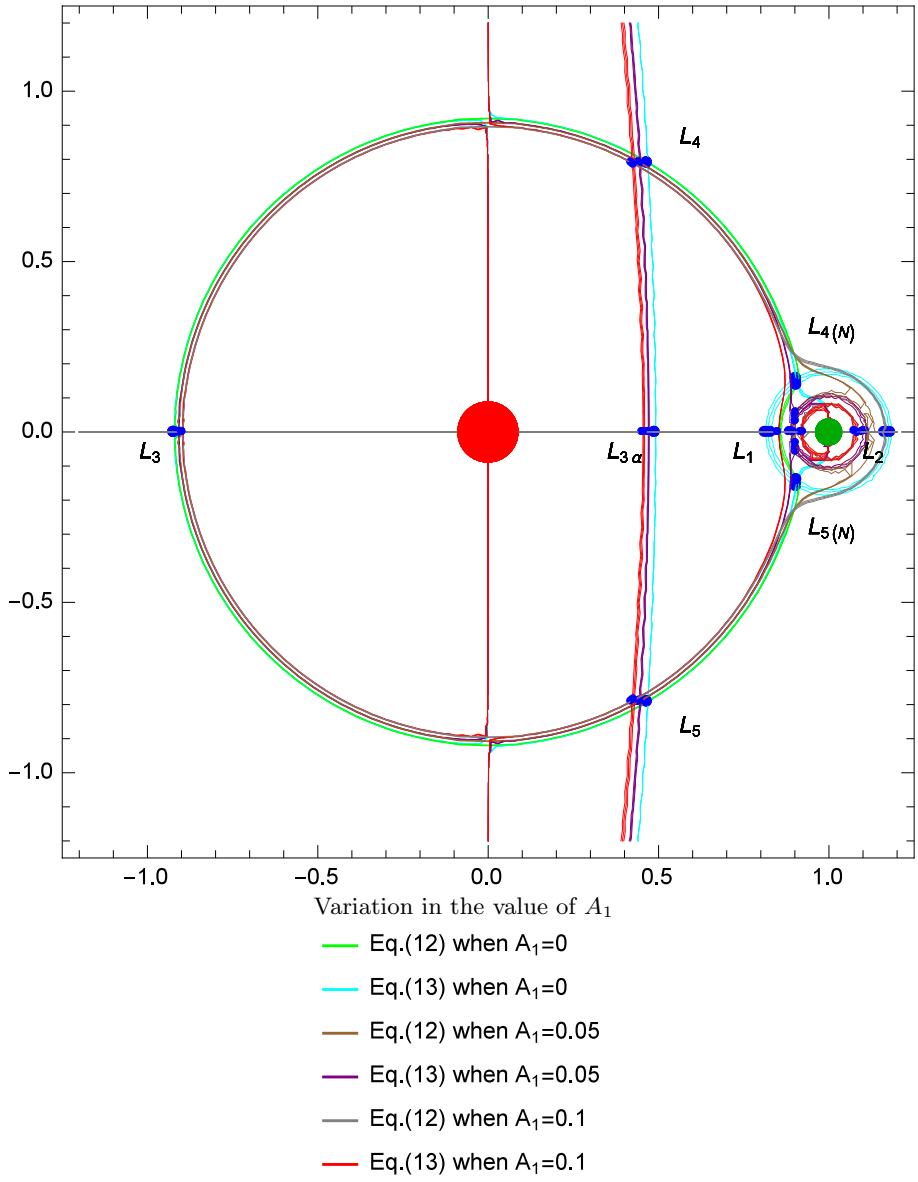

Fig. 5. The shift in the equilibrium points due to the effect of the oblateness of the second primary A_1. The blue dots represent the numerically obtained position of the planar equilibrium points.

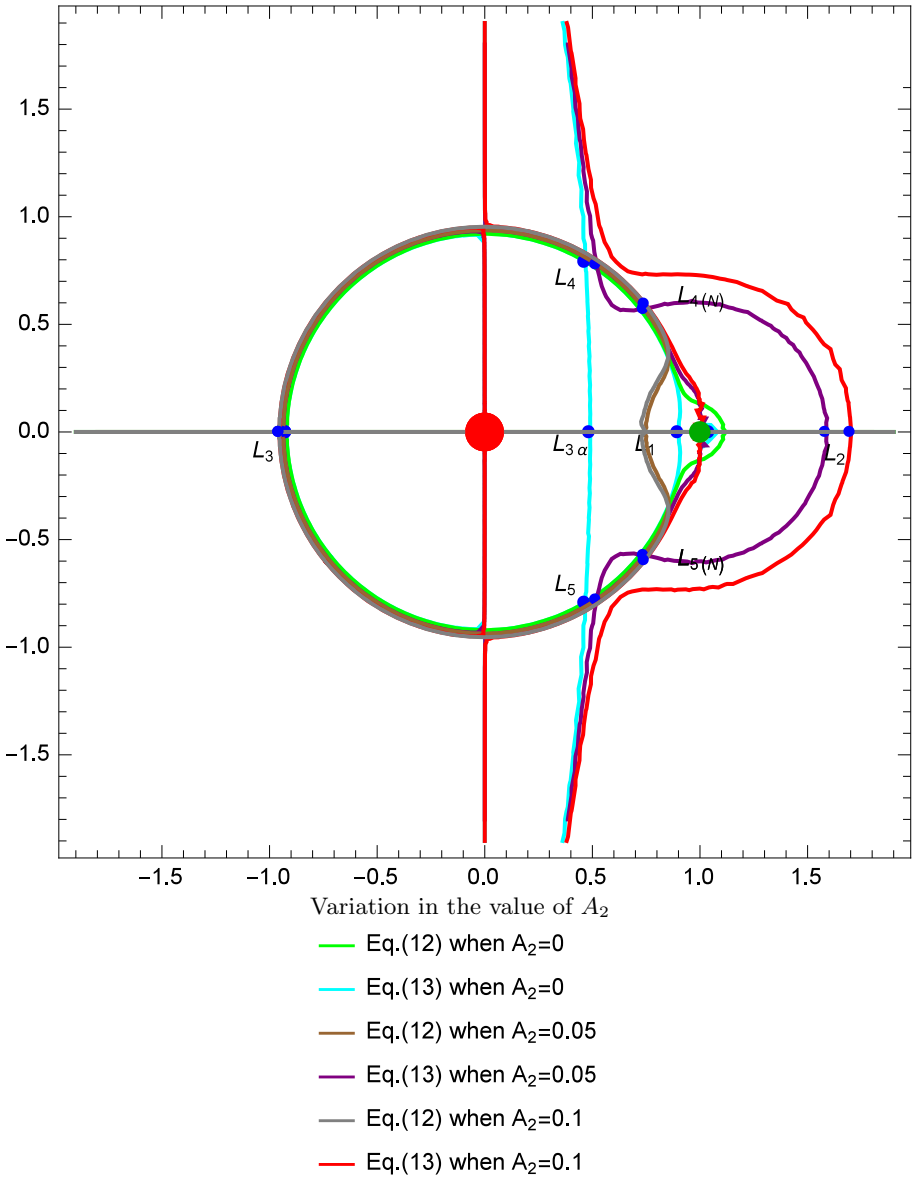

Fig. 6. The shift in the equilibrium points due to the effect of the oblateness of the second primary A_2. The blue dots represent the numerically obtained position of the planar equilibrium points.

$$\bar{r_1} = q_1^{1/3}, \quad \bar{r_2} = 1$$

Let us assume that due to the oblateness of primaries, radiation pressure and the influence of circumstellar belt, the values of $\bar{r}_1$ and $\bar{r}_2$ is given by

$$\bar{r_1} = q_1^{1/3} + \epsilon_1, \qquad \bar{r_2} = 1 + \epsilon_2. \tag{23}$$

Then, we have

$$\bar{x} = \frac{q_1^{1/3}}{2} - \mu + q_1^{1/3}\epsilon_1 - \epsilon_2, \tag{24}$$

and

$$\begin{aligned} \bar{y}^2 &= \bar{r}_1^2 - (\bar{x} - \mu)^2 \\ \Rightarrow \bar{y} &= \pm q_1^{1/3}\Big(1 - \frac{q_1^{2/3}}{4} + (2q_1^{-1/3} - q_1^{1/3})\epsilon_1 + \epsilon_2\Big)^{1/2}, \end{aligned} \tag{25}$$

Substituting equation (23)-(25) in system (19) and (20) and solving we get the values of ϵ_1 and ϵ_2 as:

$$\epsilon_1 = \frac{N_1}{Dn}, \quad \epsilon_2 = \frac{N_2}{Dn}. \tag{26}$$

where,

$$\begin{aligned} N_1 = -\Bigg[\Bigg\{1 - n^2 + \Big(\frac{B_1}{q_1^{5/3}} + \frac{B_2}{q_1^2}(1 + e\cos f)\Big)(q_1^{2/3} - 2\mu q_1^{1/3})\Bigg\}\Big(1 + \frac{5}{2}A_1(1 + e\cos f)^2 - \\ - \frac{35}{8}A_2(1 + e\cos f)^4\Big) + \mu\Big(\frac{3B_1}{2q_1^{5/3}} + \frac{B_2}{q_1^2}(1 + e\cos f)\Big)\Big(A_1(1 + e\cos f)^2. \end{aligned}$$

$$\Big.\Big(1 + \frac{15}{2}\mu\Big) - \frac{5}{8}A_2(1 + e\cos f)^4\big(2 + 21\mu\big) + 3\mu\Big)\Bigg] \tag{27}$$

$$\begin{aligned} N_2 = -\Bigg[\Big(1 - n^2 + \frac{3}{2}A_1(1 + e\cos f)^2 - \frac{15}{8}A_2(1 + e\cos f)^4\Big)\Big(q_1^{1/3} - \frac{B_1}{q_1^{4/3}}(1 - \mu)\Big) - \\ - 4\mu(q_1^{1/3} - 3\mu)\Big(\frac{3B_1}{q_1^2} + \frac{B_2}{q_1^{2/3}}(1 + e\cos f)\Big) + \frac{B_2}{q_1^{5/3}}(1 + e\cos f). \end{aligned}$$

$$\Big.\Big(1 + 2A_1(1 + e\cos f)^2\big(1 - \mu\big) - \frac{5}{2}A_2(1 + e\cos f)^4\big(1 - \mu\big)\mu\Big)\Bigg] \tag{28}$$

$$\begin{aligned} Dn = 3\Bigg[\frac{\mu}{q_1^2} - \Bigg\{\frac{1}{q_1^{1/3}} + \Big(\frac{B_1}{q_1^{4/3}}(1 - \mu) - \frac{4B_2}{3q_1^{5/3}}(1 + e\cos f)\Big)(1 - \mu)\Bigg\}. \\ \Big.\Big(1 + \frac{5}{2}A_1(1 + e\cos f)^2 - \frac{35}{8}A_2(1 + e\cos f)^4\Big)\Bigg] \end{aligned} \tag{29}$$

Hence, substituting the values of ϵ_1 and ϵ_2 in equations (24) and (25), we get the coordinates of the triangular equilibrium points.

3.2 Collinear Equilibrium points

The equilirium points lying on the $x-$axis of the plane on which the primaries are assumed to be situated are called collinear equilibrium points. The position of these equilibrium points has been obtained by adding the condition $y = 0$ to the equations (19) and (20). Thus we get reduced condition for the existence of collinear equilibrium points as:

$$f(x)=n^2\bar{x}-\left\{\frac{q_1(1-\mu)(\bar{x}+\mu)}{|\bar{x}+\mu|^3}+\frac{\mu(\bar{x}+\mu-1)}{|\bar{x}+\mu-1|^3}\left(1+\frac{3A_1}{2|\bar{x}+\mu-1|^2}\cdot(1+e\cos f)^2-\right.\right.$$
$$-\left.\frac{15A_2}{8|\bar{x}+\mu-1|^4}(1+e\cos f)^4\right)+B_1\frac{\bar{x}}{|\bar{x}|^3}+$$
$$\left.+B_2\frac{\bar{x}}{|\bar{x}|^4}(1+e\cos f)\right\}=0. \tag{30}$$

Also, in the classical studies, three collinear equilibrium points L_1, L_2 and L_3 are defined to exist in the following range:

1. L_1 lies between the bigger and the smaller primary: $-\mu < x < 1-\mu$,
2. L_2 lies to the right of the smaller primary: $x > 1-\mu$,
3. L_3 lies to the left of the bigger primary: $x < -\mu$.

However, when considering the effect of the belt, we observe that the range $-\mu < x < 1-\mu$ is further separated into two sub-ranges $-\mu < x < 0$ and $0 < x < 1-\mu$. So we shall be studying four cases:

1. L_1 lies between the bigger and the smaller primary: $0 < x < 1-\mu$,
2. L_2 lies to the right of the smaller primary: $x > 1-\mu$.
3. L_3 lies to the left of the bigger primary: $x < -\mu$,
4. $L_{3\alpha}$ lies to the right of the bigger primary: $-\mu < x$.

For each case the polynomial equation is expanded to get an idea of the number of possible real roots.

Case(i) For $\mathbf{0 < x < 1-\mu}$ In this case, we have

$$|\bar{x}+\mu|=\bar{x}+\mu, \quad |\bar{x}+\mu-1|=-(\bar{x}+\mu-1)\text{and } |\bar{x}|=x \tag{31}$$

Then,

$$f(x)=n^2\bar{x}-\left\{\frac{q_1(1-\mu)}{(\bar{x}+\mu)^2}-\frac{\mu}{(\bar{x}+\mu-1)^2}\left(1+\frac{3A_1}{2(\bar{x}+\mu-1)^2}(1+e\cos f)^2\right.\right.$$
$$\left.\left.-\frac{15A_2}{8(\bar{x}+\mu-1)^4}(1+e\cos f)^4\right)+\frac{B_1}{\bar{x}^2}+\frac{B_2}{\bar{x}^3}(1+e\cos f)\right\}=0. \tag{32}$$

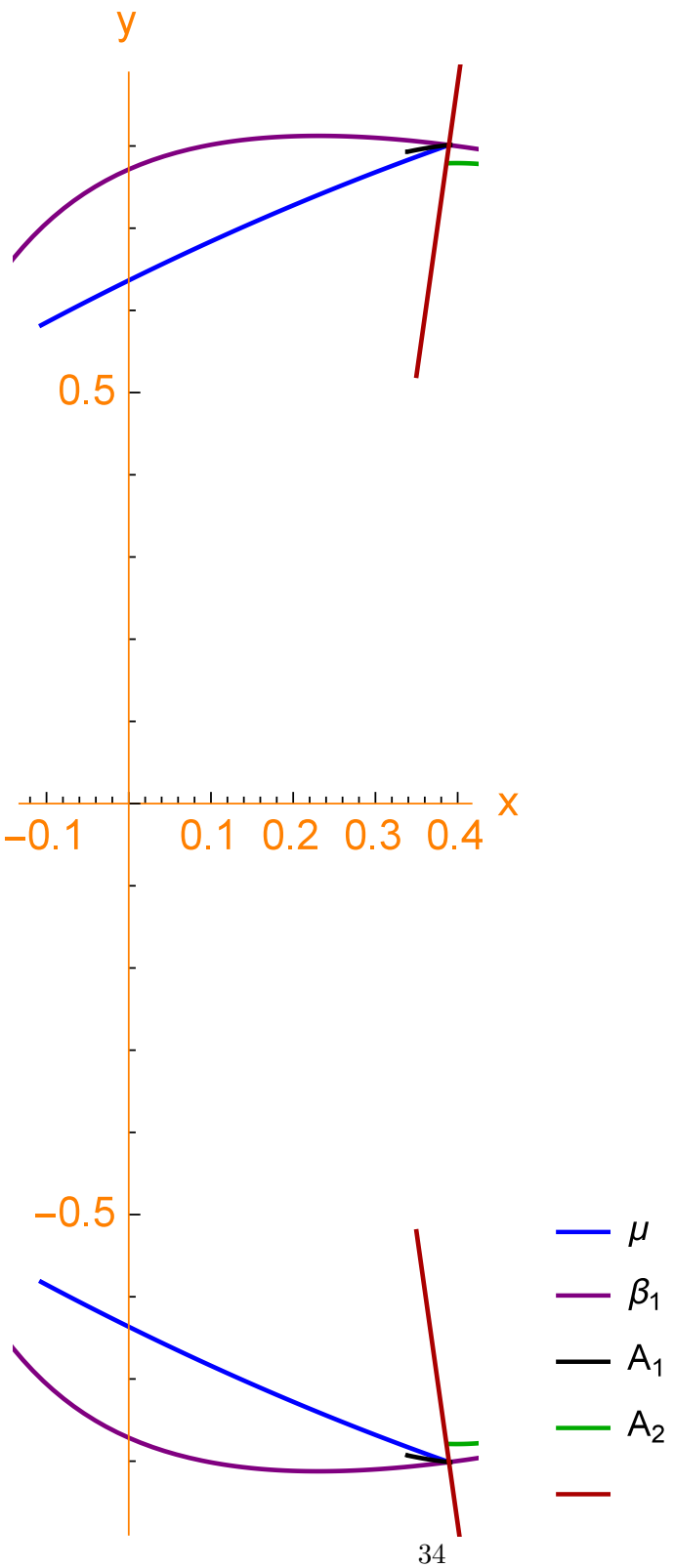

Fig. 7. The shift in the equilibrium points as calculated by analytic method, compared with respect to the different perturbing parameters

$$f'(x) = n^2 + \left\{ \frac{2q_1(1-\mu)}{(\bar{x}+\mu)^3} - \frac{2\mu}{(\bar{x}+\mu-1)^3}\left(1 + \frac{3A_1}{(\bar{x}+\mu-1)^2}(1+e\cos f)^2 \right.\right.$$
$$\left.\left. - \frac{45A_2}{8(\bar{x}+\mu-1)^4}(1+e\cos f)^4\right) + \frac{2B_1}{\bar{x}^3} + \frac{3B_2}{\bar{x}^4}(1+e\cos f)\right\} = 0.$$

we note that in this range $f'(x) > 0$, where as $f(\epsilon) \to -\infty$ and $f(1-\mu-\epsilon) \to \infty$ as $\epsilon \to 0$. Thus, in this range one collinear point, generally named as L_1 is obtained as follows:

Let

$$x + \mu - 1 = -\rho_1, \text{ where } 0 < \rho_1 << 1 \tag{33}$$

Then, equation (32) reduces to the form:

$$n^2(1-\mu-\rho_1) - \frac{q_1(1-\mu)}{(1-\rho_1)^2} + \frac{\mu}{\rho_1^2}\left(1 + \frac{3A_1(1+e\cos f)^2}{2\rho_1^2} - \frac{15A_2(1+e\cos f)^4}{8\rho_1^4}\right)$$
$$- \frac{B_1}{(1-\mu-\rho_1)^2} - \frac{B_2(1+e\cos f)}{(1-\mu-\rho_1)^3} = 0. \tag{34}$$

Simplifying, we obtain

$$\frac{\mu}{1-\mu}(1-\rho_1)^2\left(1+\frac{9}{2}A_1(1+e\cos f)^2 - \frac{75}{8}A_2(1+e\cos f)^4\right)(1-d_{c11}-d_{c12}-d_{c13})$$
$$= \rho_1^2\left(q_1 - n^2 + B_1 - B_2(1+e\cos f)\right)(1+n_{c11}-n_{c12}+n_{c13})\,; \tag{35}$$

where,

$$d_{c11} = \frac{3A_1(1+e\cos f)^2 - \frac{15}{2}A_2(1+e\cos f)^4}{1+\frac{9}{2}A_1(1+e\cos f)^2 - \frac{75}{8}A_2(1+e\cos f)^4} \tag{36}$$

$$d_{c12} = \frac{3B_1 + 4B_2(1+e\cos f)}{1+\frac{9}{2}A_1(1+e\cos f)^2 - \frac{75}{8}A_2(1+e\cos f)^4} \tag{37}$$

$$d_{c13} = \frac{n^2 + 2B_1 + 3B_2(1+e\cos f)}{1+\frac{9}{2}A_1(1+e\cos f)^2 - \frac{75}{8}A_2(1+e\cos f)^4} \tag{38}$$

$$n_{c11} = \frac{3n^2 + B_2(1+e\cos f)}{q_1 - n^2 + B_1 - B_2(1+e\cos f)} \tag{39}$$

$$n_{c12} = \frac{3n^2 + 3B_1 + 5B_2(1+e\cos f)}{q_1 - n^2 + B_1 - B_2(1+e\cos f)} \tag{40}$$

$$n_{c13} = \frac{n^2 + 2B_1 + 3B_2(1+e\cos f)}{q_1 - n^2 + B_1 - B_2(1+e\cos f)} \tag{41}$$

Taking

$$\lambda^2 = \frac{\left(1+\frac{9}{2}A_1(1+e\cos f)^2 - \frac{75}{8}A_2(1+e\cos f)^4\right)\mu}{(q_1 - n^2 + B_1 - B_2(1+e\cos f))(1-\mu)}. \tag{42}$$

For a very small value of ρ_1, $\rho_1 \approx \lambda_1$, thus we use the series expansion

$$\rho_1 = \lambda_1(1 + c_{11}\lambda_1 + c_{12}\lambda_1^2 + \cdots). \tag{43}$$

Substituting equations (42) and (43) in (35), we get the values of the coefficients c_{11} and c_{12} as follows:

$$\begin{aligned} c_{11} =& \frac{1}{2}\left(2 - d_{c11} - n_{c11}\right), \\ c_{12} =& \frac{1}{2}\left(1 - 2d_{c11} - d_{c12} + n_{c12} + c_{11}(c_{11} - 2n_{c11})\right). \end{aligned} \tag{44}$$

Thus, x-coordinate of the collinear point L_1 is given as

$$x = 1 - \mu - \rho_1, \tag{45}$$

where, ρ_1 is given using (43) and coefficients given by (44).

Case(ii) $\mathbf{x > 1-\mu}$ Here we have,

$$|\bar{x}+\mu| = \bar{x}+\mu, \quad |\bar{x}+\mu-1| = (\bar{x}+\mu-1) \quad \text{and} \quad |\bar{x}| = x \tag{46}$$

Then,

$$\begin{aligned} f(x) = n^2\bar{x} - \Bigg\{ & \frac{q_1(1-\mu)}{(\bar{x}+\mu)^2} + \frac{\mu}{(\bar{x}+\mu-1)^2}\Bigg(1 + \frac{3A_1}{2(\bar{x}+\mu-1)^2}(1+e\cos f)^2 \\ & - \frac{15A_2}{8(\bar{x}+\mu-1)^4}(1+e\cos f)^4\Bigg) + \frac{B_1}{\bar{x}^2} + \frac{B_2}{\bar{x}^3}(1+e\cos f)\Bigg\} = 0. \end{aligned} \tag{47}$$

and

$$\begin{aligned} f'(x) = n^2 + \Bigg\{ & \frac{2q_1(1-\mu)}{(\bar{x}+\mu)^3} + \frac{2\mu}{(\bar{x}+\mu-1)^3}\Bigg(1 + \frac{3A_1}{(\bar{x}+\mu-1)^2}(1+e\cos f)^2 \\ & - \frac{45A_2}{8(\bar{x}+\mu-1)^4}(1+e\cos f)^4\Bigg) + \frac{2B_1}{\bar{x}^3} + \frac{3B_2}{\bar{x}^4}(1+e\cos f)\Bigg\} = 0. \end{aligned}$$

Again we observe $f'(x) > 0$ for this range. We also find $f(1-\mu+\epsilon) \to \infty$ as $\epsilon \to 0$ and $f(\infty) \to \infty$. Thus, in this range one collinear point, generally named L_2 is obtained as follows:

Assuming

$$x + \mu - 1 = \rho_2, \text{ where } 0 < \rho_2 << 1; \tag{48}$$

equation (32) reduces to the form:

$$n^2(1-\mu+\rho_2) - \frac{q_1(1-\mu)}{(1+\rho_2)^2} - \frac{\mu}{\rho_2^2}\left(1 + \frac{3A_1(1+e\cos f)^2}{2\rho_2^2} - \frac{15A_2(1+e\cos f)^4}{8\rho_2^4}\right) - \frac{B_1}{(1-\mu+\rho_2)^2} - \frac{B_2(1+e\cos f)}{(1-\mu+\rho_2)^3} = 0. \tag{49}$$

Simplifying, we obtain

$$\frac{\mu}{1-\mu}(1+\rho_2)^2\left(1+\frac{9}{2}A_1(1+e\cos f)^2 - \frac{75}{8}A_2(1+e\cos f)^4\right)(1-d_{c11}+d_{c12}-d_{c13}) = \rho_2^2\left(n^2 - q_1 - B_1 - B_2(1+e\cos f)\right)(1+n_{c21}+n_{c22}+n_{c23}); \tag{50}$$

where,

$$n_{c21} = \frac{3n^2 + B_2(1+e\cos f)}{n^2 - q_1 - B_1 - B_2(1+e\cos f)}, \tag{51}$$

$$n_{c22} = \frac{3n^2 + 3B_1 + 5B_2(1+e\cos f)}{n^2 - q_1 - B_1 - B_2(1+e\cos f)}, \tag{52}$$

$$n_{c23} = \frac{n^2 + 2B_1 + 3B_2(1+e\cos f)}{n^2 - q_1 - B_1 - B_2(1+e\cos f)}, \tag{53}$$

and $d_{c11} - d_{c13}$ are given by (36)-(38). Taking

$$\lambda^2 = \frac{\left(1 + \frac{9}{2}A_1(1+e\cos f)^2 - \frac{75}{8}A_2(1+e\cos f)^4\right)\mu}{(n^2 - q_1 - B_1 - B_2(1+e\cos f))(1-\mu)}. \tag{54}$$

For a very small value of ρ_2, $\rho_2 \approx \lambda_2$, thus we use the series expansion

$$\rho_2 = \lambda_2(1 + c_{21}\lambda_2 + c_{22}\lambda_2^2 + \cdots). \tag{55}$$

Substituting equations (54) and (55) in (50), we get the values of the coefficients c_{21} and c_{22} as follows:

$$c_{21} = \frac{1}{2}\left(2 - d_{c11} + n_{c21}\right).$$

$$c_{22} = \frac{1}{2}\left(1 - 2d_{c11} + d_{c12} + n_{c22} + c_{21}(c_{21} + 2n_{c21})\right). \tag{56}$$

Thus, x-coordinate of the collinear point L_2 is given as

$$x = 1 - \mu + \rho_2, \tag{57}$$

where, ρ_2 is given using (55) and coefficients are given by (56).

Case(iii) $\mathbf{x} < -\mu$
In this case, we have

$$|x+\mu| = -(x+\mu), \quad |x+\mu-1| = -(x+\mu-1) \text{ and } |x| = -x \tag{58}$$

Then, from equation (30), we have

$$f(x) = n^2\bar{x} + \left\{ \frac{q_1(1-\mu)}{(\bar{x}+\mu)^2} + \frac{\mu}{(\bar{x}+\mu-1)^2}\left(1 + \frac{3A_1}{2(\bar{x}+\mu-1)^2}(1+e\cos f)^2 - \frac{15A_2}{8(\bar{x}+\mu-1)^4}(1+e\cos f)^4\right) + \frac{B_1}{\bar{x}^2} - \frac{B_2}{\bar{x}^3}(1+e\cos f)\right\} = 0. \tag{59}$$

and

$$f'(x) = n^2 - \left\{ \frac{2q_1(1-\mu)}{(\bar{x}+\mu)^3} + \frac{2\mu}{(\bar{x}+\mu-1)^3}\left(1 + \frac{3A_1}{(\bar{x}+\mu-1)^2}(1+e\cos f)^2 - \frac{45A_2}{8(\bar{x}+\mu-1)^4}(1+e\cos f)^4\right) + \frac{2B_1}{\bar{x}^3} - \frac{3B_2}{\bar{x}^4}(1+e\cos f)\right\} = 0.$$

Again we observe $f'(x) > 0$ for this range. We also find $f(-\infty) \to -\infty$ and $f(-\mu-\epsilon) \to \infty$ as $\epsilon \to 0$. Thus, in this range one collinear point, generally named L_3 is obtained as follows:
We take

$$x + \mu = -\rho_3, \text{ where } 0 < \rho_3 << 1. \tag{60}$$

Then, equation (59) reduces to the form:

$$-n^2(\mu+\rho_3) + \left\{ \frac{q_1(1-\mu)}{\rho_3^2} + \frac{\mu}{(1+\rho_3)^2}\left(1 + \frac{3A_1}{2(1+\rho_3)^2}(1+e\cos f)^2 - \frac{15A_2}{8(1+\rho_3)^4}(1+e\cos f)^4\right) + \frac{B_1}{(\mu+\rho_3)^2} - \frac{B_2}{(\mu+\rho_3)^3}(1+e\cos f)\right\} = 0. \tag{61}$$

Simplifying, we obtain

$$\frac{\mu}{1-\mu} = \frac{q_1 + (3B_1 - 4B_2(1+e\cos f))\rho_3^2 - (n^2 + 2B_1 - 3B_2(1+e\cos f))\rho^3}{\left[n^2 - 1 - \frac{3A_1}{2}(1+e\cos f)^2 + \frac{15A_2}{8}(1+e\cos f)^4 - B_1 + B_2(1+e\cos f) + \left(3n^2 + 3A_1(1+e\cos f)^2 - \frac{15A_2}{2}(1+e\cos f)^4 - B_2(1+e\cos f)\right)\rho_3 + \left(3n^2 + 3B_1 - 5B_2(1+e\cos f)\right)\rho_3^2 + \left(n^2 + 2B_1 - 3B_2(1+e\cos f)\right)\rho_3^3\right]} \tag{62}$$

Thus taking

$$\alpha = \rho_3 - 1,\ q_1 = 1 - \beta_1 \text{ and } n^2 = 1 - \delta_n; \tag{63}$$

equation (76) is represented as

$$\frac{\mu}{1-\mu} = -\frac{N_1}{D_1}. \tag{64}$$

Here, the numerator and denominator are

$$\begin{aligned} N_1 =& 4(\beta_1 - \delta_n - B_1 + B_2(1 + e\cos f)) + (12 + 4\beta_1 - 16\delta_n - 4B_1)\alpha \\ &+ (24 + \beta_1 - 25\delta_n + 11B_1 - 23B_2(1 + e\cos f))\alpha^2 \\ &+ (19 - 19\delta_n + 20B_1 - 33B_2(1 + e\cos f))\alpha^3 + \cdots \end{aligned} \tag{65}$$

$$\begin{aligned} D_1 =& 7 - 8\delta_n + \frac{3A_1}{2}(1+e\cos f)^2 - \frac{45A_2}{8}(1+e\cos f)^4 + 4B_1 - 8B_2(1+ e\cos f) \\ &+ \left(26 - 28\delta_n + \frac{12A_1}{2}(1+e\cos f)^2 - \frac{75A_2}{4}(1+ e\cos f)^4 + 20B_1 - 36B_2(1+ e\cos f)\right)\alpha \\ &+ \left(37 - 38\delta_n + \frac{15A_1}{2}(1+e\cos f)^2 - \frac{165A_2}{8}(1+e\cos f)^4 + 37B_1 - 62B_2(1+e\cos f)\right)\alpha^2 \\ &+ \left(25 - 25\delta_n + \frac{6A_1}{2}(1+e\cos f)^2 - \frac{15A_2}{2}(1+e\cos f)^4 + 32B_1 - 51B_2(1+e\cos f)\right)\alpha^3 \end{aligned} \tag{66}$$

Then, from equation (64)

$$\mu = -\frac{N_1}{D_1 - N_1}. \tag{67}$$

We get

$$\begin{aligned} -\frac{\mu_1}{\alpha} =& \frac{12}{7} + \frac{20}{49}\beta_1 - \frac{8}{49}\delta_n - \frac{18A_1}{49}(1+e\cos f)^2 + \frac{135A_2}{98}(1+e\cos f)^4 - \frac{68}{49}B_1 \\ &+ \frac{88}{49}B_2(1+e\cos f) - \left(\frac{37}{49}\beta_1 - \frac{37}{49}\delta_n + \frac{36A_1}{49}(1+e\cos f)^2 - \frac{90A_2}{49}(1+e\cos f)^4\right. \\ &\left. + \frac{23}{49}B_1 - \frac{43}{49}B_2(1+e\cos f)\right)\alpha - \left(\frac{23}{49} - \frac{82}{343}\beta_1 - \frac{1}{49}\delta_n - \frac{285A_1}{686}(1+e\cos f)^2\right. \\ &\left. + \frac{4275A_2}{2744}(1+e\cos f)^4 - \frac{354}{343}B_1 + \frac{531}{343}B_2(1+e\cos f)\right)\alpha^2 + \cdots \end{aligned} \tag{68}$$

where,

$$\mu_1 = \mu + \frac{4(\beta_1 - \delta_n - B_1 + B_2(1 + e\cos f))}{7}. \tag{69}$$

The first approximation to a solution for α in linear terms is given as

$$\alpha=\alpha_0=\frac{-\mu_1}{\frac{12}{7}+\frac{20}{49}\beta_1-\frac{8}{49}\delta_n-\frac{18A_1}{49}(1+e\cos f)^2+\frac{135A_2}{98}(1+e\cos f)^4 \\ -\frac{68}{49}B_1+\frac{88}{49}B_2(1+e\cos f)}=-\frac{7}{12}\mu_1. \quad (70)$$

Then, the next approximation for α is obtained as:

$$\begin{aligned}\alpha = \quad & \alpha_0 \\ & -\frac{\left(\begin{array}{c}\frac{37}{49}\beta_1-\frac{37}{49}\delta_n+\frac{36A_1}{49}(1+e\cos f)^2-\frac{90A_2}{49}(1+e\cos f)^4 \\ +\frac{23}{49}B_1-\frac{43}{49}B_2(1+e\cos f)\end{array}\right)}{\left(\begin{array}{c}\frac{12}{7}+\frac{20}{49}\beta_1-\frac{8}{49}\delta_n-\frac{18A_1}{49}(1+e\cos f)^2+\frac{135A_2}{98}(1+e\cos f)^4 \\ -\frac{68}{49}B_1+\frac{88}{49}B_2(1+e\cos f)\end{array}\right)}\alpha_0^2 \\ & +\left[2\left(\frac{\left(\begin{array}{c}\frac{37}{49}\beta_1-\frac{37}{49}\delta_n+\frac{36A_1}{49}(1+e\cos f)^2-\frac{90A_2}{49}(1+e\cos f)^4 \\ +\frac{23}{49}B_1-\frac{43}{49}B_2(1+e\cos f)\end{array}\right)}{\left(\begin{array}{c}\frac{12}{7}+\frac{20}{49}\beta_1-\frac{8}{49}\delta_n-\frac{18A_1}{49}(1+e\cos f)^2+\frac{135A_2}{98}(1+e\cos f)^4 \\ -\frac{68}{49}B_1+\frac{88}{49}B_2(1+e\cos f)\end{array}\right)}\right)^2\right. \\ & \left.+\frac{\left(\begin{array}{c}\frac{23}{49}-\frac{82}{343}\beta_1-\frac{1}{49}\delta_n-\frac{285A_1}{686}(1+e\cos f)^2+\frac{4275A_2}{2744}(1+e\cos f)^4 \\ +\frac{354}{343}B_1+\frac{531}{343}B_2(1+e\cos f)\end{array}\right)}{\left(\begin{array}{c}\frac{12}{7}+\frac{20}{49}\beta_1-\frac{8}{49}\delta_n-\frac{18A_1}{49}(1+e\cos f)^2+\frac{135A_2}{98}(1+e\cos f)^4 \\ -\frac{68}{49}B_1+\frac{88}{49}B_2(1+e\cos f)\end{array}\right)}\right]\alpha_0^3+\cdots\end{aligned} \quad (71)$$

Thus, x-coordinate of the collinear point L_3 is given as

$$x = 1-\mu+\alpha. \quad (72)$$

Case(iv) $-\mu < \mathbf{x} < \mathbf{0}$

In this case, we have

$$|x+\mu|=(x+\mu), \quad |x+\mu-1|=-(x+\mu-1) \text{ and } |x|=-x \quad (73)$$

Then, from equation (30), we have

$$f(x) = n^2\bar{x} - \left\{ \frac{q_1(1-\mu)}{(\bar{x}+\mu)^2} + \frac{\mu}{(\bar{x}+\mu-1)^2}\left(1 + \frac{3A_1}{2(\bar{x}+\mu-1)^2}\,(1+e\cos f)^2 \right.\right.$$
$$\left.\left. - \frac{15A_2}{8(\bar{x}+\mu-1)^4}\,(1+e\cos f)^4\right) + \frac{B_1}{\bar{x}^2} + \frac{B_2}{\bar{x}^3}\,(1+e\cos f)\right\} = 0. \tag{74}$$

and

$$f'(x) = n^2 - \left\{ -\frac{2q_1(1-\mu)}{(\bar{x}+\mu)^3} + \frac{2\mu}{(\bar{x}+\mu-1)^3}\left(1 + \frac{3A_1}{(\bar{x}+\mu-1)^2}\,(1+e\cos f)^2 \right.\right.$$
$$\left.\left. - \frac{45A_2}{8(\bar{x}+\mu-1)^4}\,(1+e\cos f)^4\right) + \frac{2B_1}{\bar{x}^3} - \frac{3B_2}{\bar{x}^4}\,(1+e\cos f)\right\} = 0.$$

Again we observe $f'(x) > 0$ for this range. We also find $f(-\mu+\epsilon) \to -\infty$ and $f(-\epsilon) \to \infty$ as $\epsilon \to 0$. Thus, in this range also one collinear point may exist which is named $L_{3\alpha}$ by assuming Let

$$x + \mu = \rho_4, \text{ where } 0 < \rho_4 << 1 \tag{75}$$

Then, equation (74) reduces to the form:

$$n^2(-\mu+\rho_4) + \left\{ \frac{q_1(1-\mu)}{\rho_4^2} + \frac{\mu}{(\rho_4-1)^2}\left(1 + \frac{3A_1}{2(\rho_4-1)^2}\,(1+e\cos f)^2 \right.\right.$$
$$\left.\left. - \frac{15A_2}{8(\rho_4-1)^4}\,(1+e\cos f)^4\right) - \frac{B_1}{(-\mu+\rho_4)^2} - \frac{B_2}{(-\mu+\rho_4)^3}\,(1+e\cos f)\right\} = 0. \tag{76}$$

Simplifying, we obtain

$$\frac{\mu}{1-\mu} = \frac{\begin{array}{c} q_1 - 2q_1\rho_4 + (q_1 + 3B_1 - 4B_2(1+e\cos f))\rho_4^2 + (n^2 - 8B_1 + 11B_2(1+e\cos f))\rho_4^3 \\ -(2n^2 - 7B_1 + 10B_2(1+e\cos f))\rho_4^4 + (n^2 - 2B_1 + 3B_2(1+e\cos f))\rho_4^5 \end{array}}{\left[\begin{array}{l} n^2 - 1 - \frac{3A_1}{2}(1+e\cos f)^2 + \frac{15A_2}{8}(1+e\cos f)^4 - B_1 + B_2(1+e\cos f) \\ +\left(3n^2 + 3A_1(1+e\cos f)^2 - \frac{15A_2}{2}(1+e\cos f)^4 - B_2(1+e\cos f)\right)\rho_3 \\ +\left(3n^2 + 3B_1 - 5B_2(1+e\cos f)\right)\rho_3^2 + \left(n^2 + 2B_1 - 3B_2(1+e\cos f)\right)\rho_3^3 \end{array}\right]}. \tag{77}$$

Now taking

$$\alpha^* = \rho_4 + 1,\ q_1 = 1 - \beta_1 \text{ and } n^2 = 1 - \delta_n; \tag{78}$$

equation (77) is represented as

$$\frac{\mu}{1-\mu}=\frac{N_2}{7D_2}. \tag{79}$$

Here, the numerator and denominator are

$$\begin{aligned}N_2=&4(\delta_n-\beta_1+5B_1-7B_2(1+e\cos f))+(12+4\beta_1-16\delta_n-68B_1+96B_2(1+e\cos f))\alpha^*\\&-(24+\beta_1-25\delta_n-89B_1+127B_2(1+e\cos f))(\alpha^*)^2\\&+(19-19\delta_n-56B_1+81B_2(1+e\cos f))(\alpha^*)^3\\&-(7-7\delta_n-17B_1+25B_2(1+e\cos f))(\alpha^*)^4+(1-\delta_n-2B_1+3B_2(1+e\cos f))(\alpha^*)^5,\end{aligned} \tag{80}$$

$$\begin{aligned}D_2=&1-\frac{8\delta_n}{7}+\frac{3A_1}{14}(1+e\cos f)^2-\frac{45A_2}{56}(1+e\cos f)^4-4B_1+\frac{40}{7}B_2(1+e\cos f)\\&-\left(\frac{26}{7}-4\delta_n+\frac{12A_1}{14}(1+e\cos f)^2-\frac{75A_2}{28}(1+e\cos f)^4-\frac{92}{7}B_1+\frac{132}{7}B_2(1+e\cos f)\right)\alpha^*\\&+\left(\frac{37}{7}-\frac{38\delta_n}{7}+\frac{15A_1}{14}(1+e\cos f)^2-\frac{165A_2}{56}(1+e\cos f)^4\right.\\&\qquad\left.-\frac{115}{7}B_1+\frac{166}{7}B_2(1+e\cos f)\right)(\alpha^*)^2\\&-\left(\frac{25}{7}-\frac{25\delta_n}{7}+\frac{6A_1}{14}(1+e\cos f)^2-\frac{15A_2}{14}(1+e\cos f)^4-\frac{68}{7}B_1+\frac{99}{7}B_2(1+e\cos f)\right)(\alpha^*)^3\\&+\left(\frac{8}{7}-\frac{8}{7}\delta_n-\frac{19}{7}B_1+4B_2(1+e\cos f)\right)(\alpha^*)^4\\&2-\left(\frac{1}{7}(1-\delta_n)-\frac{2}{7}B_1+\frac{3}{7}B_2(1+e\cos f)\right)(\alpha^*)^5.\end{aligned} \tag{81}$$

We get

$$\begin{aligned}-\frac{\mu_2}{\alpha^*}=&\frac{12}{7}-\frac{76}{49}\beta_1+\frac{88}{49}\delta_n-\frac{18A_1}{49}(1+e\cos f)^2+\frac{135A_2}{98}(1+e\cos f)^4-\frac{380}{49}B_1\\&-\frac{536}{49}B_2(1+e\cos f)+\left(\frac{144}{49}-\frac{989}{343}\beta_1+\frac{1227}{343}\delta_n-\frac{180A_1}{343}(1+e\cos f)^2\right.\\&+\frac{990A_2}{343}(1+e\cos f)^4-\frac{536}{343}B_1-\frac{757}{343}B_2(1+e\cos f)\Big)\alpha^*+\left(\frac{1567}{343}-\frac{10930}{2401}\beta_1\right.\\&-\frac{2207}{343}\delta_n-\frac{1461A_1}{4802}(1+e\cos f)^2+\frac{82395A_2}{19208}(1+e\cos f)^4\\&\left.-\frac{65122}{2401}B_1-\frac{9179}{2401}B_2(1+e\cos f)\right)(\alpha^*)^2+\cdots;\end{aligned} \tag{82}$$

where,

$$\mu_2=\frac{\mu}{1-\mu}+\frac{4}{7}(\delta_n-\beta_1+5B_1-7B_2(1+e\cos f)). \tag{83}$$

The first approximation to a solution for α in linear terms is given as

$$\alpha^* = \alpha_0^* = \frac{\mu_2}{\left[\begin{array}{c}\frac{12}{7} - \frac{76}{49}\beta_1 + \frac{88}{49}\delta_n - \frac{18A_1}{49}(1+e\cos f)^2 \\ + \frac{135A_2}{98}(1+e\cos f)^4 - \frac{380}{49}B_1 - \frac{536}{49}B_2(1+e\cos f)\end{array}\right]} = \frac{7}{12}\mu_1. \quad (84)$$

Then, the next approximation for α is obtained as:

$$\begin{aligned}
&\alpha^* \\
&= \alpha_0^* \\
&\quad - \left[\frac{1}{Dn^*}\left(\frac{144}{49} - \frac{989}{343}\beta_1 + \frac{1227}{343}\delta_n - \frac{180A_1}{343}(1+e\cos f)^2 + \frac{990A_2}{343}(1+e\cos f)^4\right.\right. \\
&\quad \left.\left. - \frac{536}{343}B_1 - \frac{757}{343}B_2(1+e\cos f)\right)\right](\alpha_0^*)^2 \\
&\quad + \left[\frac{2}{(Dn^*)^2}\left(\frac{144}{49} - \frac{989}{343}\beta_1 + \frac{1227}{343}\delta_n - \frac{180A_1}{343}(1+e\cos f)^2 + \frac{990A_2}{343}(1+e\cos f)^4\right.\right. \\
&\quad \left.\left. - \frac{536}{343}B_1 - \frac{757}{343}B_2(1+e\cos f)\right)^2\right. \\
&\quad \left. - \frac{1}{Dn^*}\left(\frac{1567}{343} - \frac{10930\beta_1}{2401} - \frac{2207\delta_n}{343} - \frac{1461A_1(1+e\cos f)^2}{4802} + \frac{82395A_2(1+e\cos f)^4}{19208}\right.\right. \\
&\quad \left.\left. - \frac{65122B_1}{2401} - \frac{9179B_2(1+e\cos f)}{2401}\right)\right](\alpha_0^*)^3 + \cdots \quad (85)
\end{aligned}$$

where,

$$\begin{aligned}
Dn^* &= \frac{12}{7} - \frac{76}{49}\beta_1 + \frac{88}{49}\delta_n - \frac{18A_1}{49}(1+e\cos f)^2 + \frac{135A_2}{98}(1+e\cos f)^4 \\
&\quad - \frac{380}{49}B_1 - \frac{536}{49}B_2(1+e\cos f) \quad (86)
\end{aligned}$$

Thus, x-coordinate of the collinear point $L_{3\alpha}$ is given as

$$x = -1 - \mu + \alpha^*. \quad (87)$$

In this section the equilibrium point for the model has been analytically derived as a function of μ, e and the factors of perturbing forces. Though in the previous section we had numerically observed existence of two pairs of non-collinear equilibrium points, analytically the position of the triangular equilibrium point was derived. However, analytical methods also verify the existence of four collinear equilibrium points.

Figures 7-10 graphically explore the dependence of the position of equilibrium points on the various perturbing forces as well as the mass factor μ.

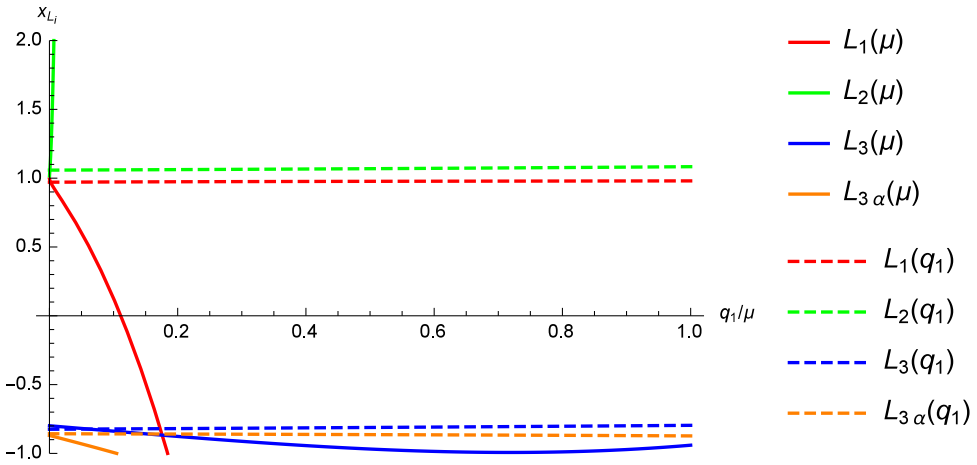

Fig. 8. The shift in the x-coordinate of collinear equilibrium points as calculated by analytic method, compared with respect to the parameters: mass ratio μ and mass reduction factor q_1

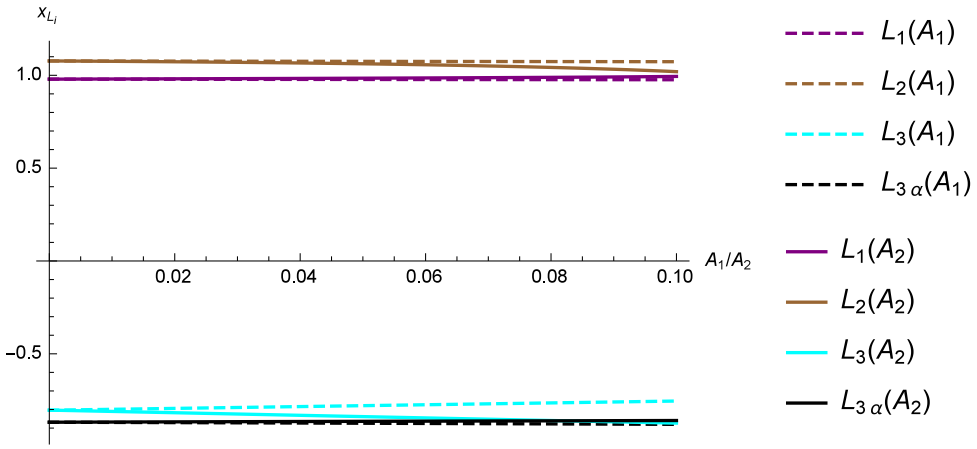

Fig. 9. The shift in the x-coordinate of collinear equilibrium points as calculated by analytic method, compared with respect to the oblateness parameters of the second primary: A_1 and A_2

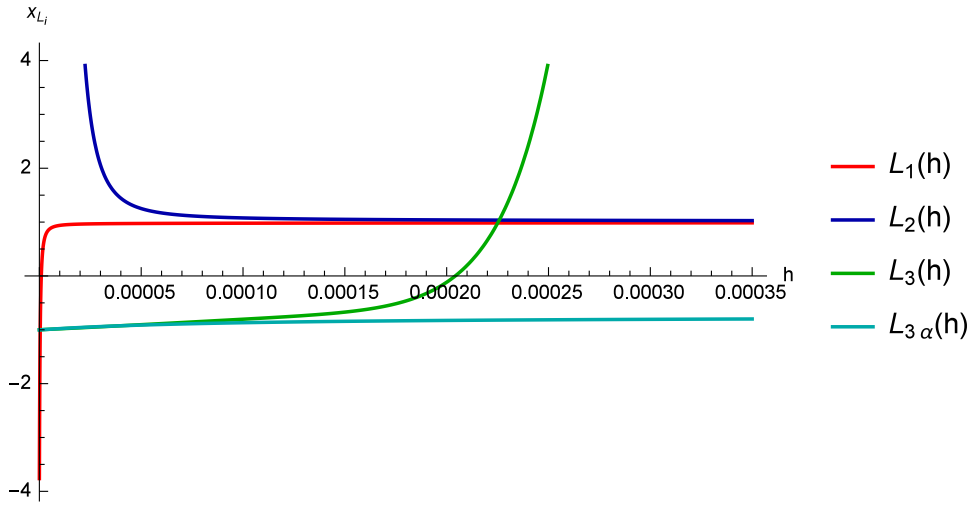

Fig. 10. The shift in the x-coordinate of collinear equilibrium points as calculated by analytic method, compared with respect to the parameters due to the circumstellar belt: B_1 and B_2

In figure 7 the shift in the position of the triangular equilibrium points with the change in the various parameters is observed. When one of the parameters is varied, the others are taken as constant according to Sun-Jupiter system. The variation of the parameters are as follows: $0 \leq \mu \leq 0.5$, $1 \geq q \geq 0.6$, $0 \leq h \leq 0.0003$, $0 \leq A_1, A_2 \leq 0.1$ respectively. It was observed that variation in each factor have effect on the triangular points. They are most affected by the radiation factor q_1, then mass parameter μ and then the circumstellar belt. Figure 8 shows the shift in the $x-$coordinate of the four collinear equilibrium points with the change in the values of μ and q_1. The collinear points especially L_1 and L_2 show drastic shift in their position with change in the value of μ. The radiation factor q_1 does not show any effect on the position of the collinear points. Figure 9 is the representation of the $x-$coordinate as the function of the oblateness parameters A_1 and A_2. It shows slight effect on the position of the points. L_2 is shifted towards origin whereas L_3 is shifted away from it. Figure 10 shows the shift with respect to the thickness of the circumstellar belt. All the collinear points were found to be dependent on the circumstellar belt factor which in turn is dependent on the thickness of the belt.

4 Fractal Basin

In this section, multi-variate version of Newton-Raphson's method is employed to get the Basin of attraction of the planar equilibrium points. Fractal basin of attraction of a point(attractor) is referred to the region from which each point after a number of iteration tends toward the point. Studying the structure of such region for roots of non-linear equation, it was found that they have

fractus boundaries. The main use of these basin of attraction is in choice of initial point for orbits around the equilibrium point. If the initial point is chosen from inside the region of attraction, the possibility of getting stable orbit is high, however the initial point chosen among the boundary values shows chaotic behavior. For study of basin of attraction of equilibrium points of dynamical models various methods are available [Kalvouridis & Gousidou-Koutita (2012)] studied the modified Broyden's method and Newton-Raphson method and proved that the Newton-Raphson's method is more appropriate for dynamical systems as they show much better rate of convergence.

The iterative scheme for each planar equilibrium point in the $\bar{x}\bar{y}$ plane, is as follows:

$$\bar{x}_{n+1} = \bar{x}_n - \left(\frac{\Omega_{\bar{x}}\Omega_{\bar{y}\bar{y}} - \Omega_y \Omega_{\bar{x}\bar{y}}}{\Omega_{\bar{x}\bar{x}}\Omega_{\bar{y}\bar{y}} - \Omega^2_{\bar{x}\bar{y}}} \right)_{(\bar{x}_n, \bar{y}_n)};$$

$$\bar{y}_{n+1} = \bar{y}_n + \left(\frac{\Omega_{\bar{x}}\Omega_{\bar{y}\bar{x}} - \Omega_{\bar{y}}\Omega_{\bar{y}\bar{y}}}{\Omega_{\bar{x}\bar{x}}\Omega_{\bar{y}\bar{y}} - \Omega^2_{\bar{x}\bar{y}}} \right)_{(\bar{x}_n, \bar{y}_n)};$$

where,

$$\Omega_{\bar{x}} = \frac{1}{1+e\cos f}\left[\bar{x} - \frac{1}{n^2}\left\{\frac{q_1(1-\mu)(\bar{x}+\mu)}{\bar{r}_1^3} + \frac{\mu(\bar{x}+\mu-1)}{\bar{r}_2^3}\left(1 + \frac{3A_1}{2\bar{r}_2^2}(1+e\cos f)^2 - \frac{15A_2}{8\bar{r}_2^4}(1+e\cos f)^4\right) + \frac{2ch\pi(a-b)}{ab}\frac{\bar{x}}{\bar{r}^3} + \frac{3ch\pi}{8}\log\frac{a}{b}\frac{\bar{x}}{\bar{r}^4}(1+e\cos f)\right\}\right], \tag{88}$$

$$\Omega_{\bar{y}} = \frac{1}{1+e\cos f}\left[\bar{y} - \frac{1}{n^2}\left\{\frac{q_1(1-\mu)\bar{y}}{\bar{r}_1^3} + \frac{\mu\bar{y}}{\bar{r}_2^3}\left(1 + \frac{3A_1}{2\bar{r}_2^2}(1+e\cos f)^2 - \frac{15A_2}{8\bar{r}_2^4}(1+e\cos f)^4\right) + \frac{2ch\pi(a-b)}{ab}\frac{\bar{y}}{\bar{r}^3} + \frac{3ch\pi}{8}\log\frac{a}{b}\frac{\bar{y}}{\bar{r}^4}(1+e\cos f)\right\}\right]. \tag{89}$$

And $\Omega_{\bar{x}\bar{x}}$, $\Omega_{\bar{y}\bar{y}}$, $\Omega_{\bar{x}\bar{y}}$ are the second order derivatives of the potential function Ω.

Different colors have been used to depict the basin of attraction of the different equilibrium points. The color coded diagrams in the $\bar{x}\bar{y}$-plane are plotted. Figure 11 shows the Newton-Raphson basins of attraction on the configuration $\bar{x}\bar{y}$-plane varying the values of eccentricity e and radiation pressure factor q_1, whereas Figure 12 shows the effect of the variation of e and q_1 when the influence of belt is also considered. The comparison of the two figures shows that the circumstellar belt is affecting the basin of convergence. In these figures the color code is as follows: the basin of convergence of L_1 is colored Green, L_2 is Cyan, L_3 is Yellow, $L_{3\alpha}$ is White, L_4 is Red, L_5 is Magenta, $L_{4(N)}$ is Dark red, $L_{5(N)}$ is Purple. Comparing sub-figure 11(c) and (d), it was foud that basin of attraction of L_5 reduces with decrease in the value of radiation pressure, whereas the basin of attraction of L_2 and L_3 expands; similar

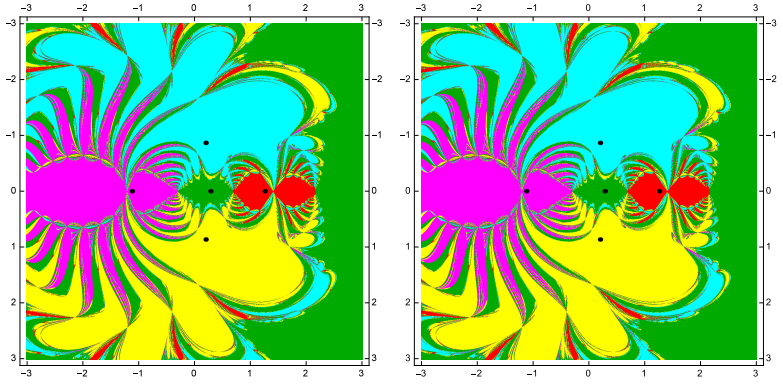

(a) $\mu = 0.3,\ e = 0,\ q_1 = 1$ (b) $\mu = 0.3,\ e = 0.01,\ q_1 = 1$

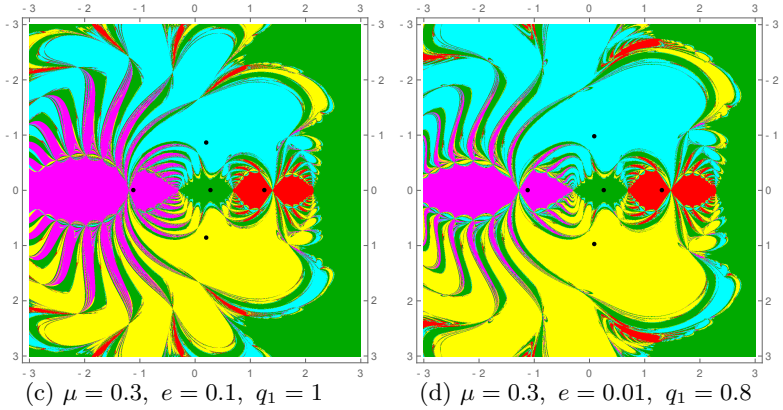

(c) $\mu = 0.3,\ e = 0.1,\ q_1 = 1$ (d) $\mu = 0.3,\ e = 0.01,\ q_1 = 0.8$

Fig. 11. Fractal basin on the $\bar{x}\bar{y}-$plane, when the circumstellar belt is neglected

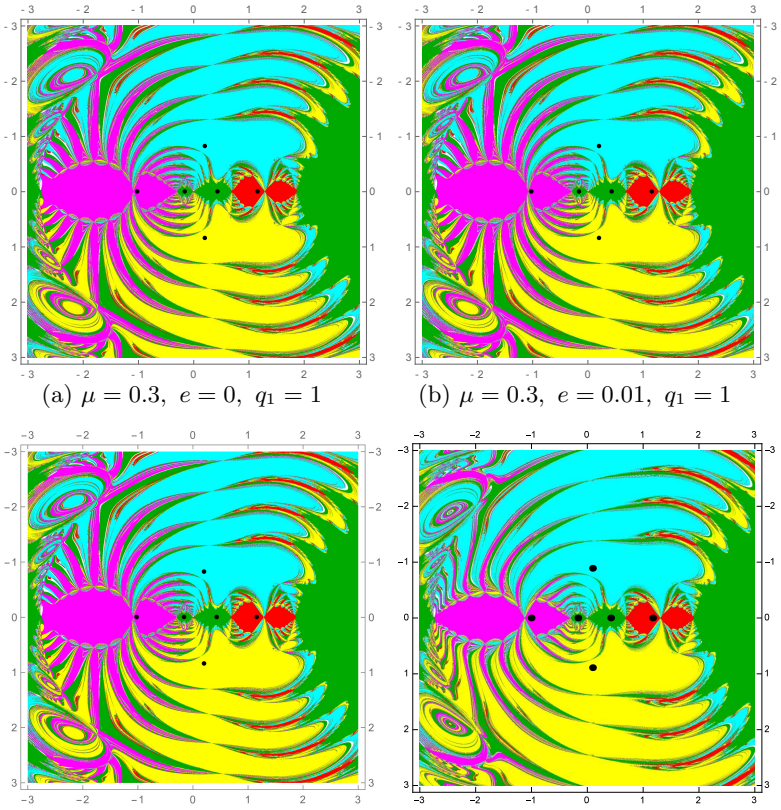

(a) $\mu = 0.3,\ e = 0,\ q_1 = 1$ (b) $\mu = 0.3,\ e = 0.01,\ q_1 = 1$

(c) $\mu = 0.3,\ e = 0.1,\ q = 1$ (d) $\mu = 0.3,\ e = 0.1,\ q = 0.8$

Fig. 12. Fractal basin on the $\bar{x}\bar{y}-$plane, considering the effect of circumstellar belt

phenomenon is observed for sub-figures 12(c) and (d). Comparing sub-figures 11(a), (b) and (c), we observe that the increase in the value of eccentricity of the orbits e is not effecting the structure or extend of the basin of convergence of the equilibrium points, similar was the observation about sub-figures 12(a), (b) and (c). Again comparing the figures 11 and 12, we observe the circumstellar belt is effecting the extend as well as the structure of the basin of attraction of the various equilibrium points. The size of the basin for L_4 and L_5 decreases under the effect of circumstellar belt, whereas the basin for L_1, L_2 and L_3 changes shape and becomes elongated and the boundaries are more fractus. The fractal basin for $L_{3\alpha}$, $L_{4(N)}$ and $L_{5(N)}$ becomes visible though the regions are very limited and highly fractal in nature.

Figure 13 is representation of the fractal basin of attraction for Sun-Jupiter system. The two sub-figures highlight the difference due to circumstellar belt. The effect is the same as discussed above.

Conclusions and Discussions

A system of two massive objects orbiting in elliptical orbits and surrounded by a circumstellar belt is modeled in this problem. It was assumed that the potential due to the circumstellar belt is defined by Power Law Profile, the largest primary is illuminating and the second primary is oblate. The equation of motion of the system in the rotating, pulsating barycentric frame of reference is derived.

Firstly, numerical methods are employed to apply this model on Sun-Jupiter system and obtain the number and position of equilibrium points. When the perturbing forces are considered, the presence of eight equilibrium points was detected, five of which equilibrium points are analogues to the classically obtained Lagrangian equilibrium points L_1, L_2, L_3 (collinear points), L_4 and L_5(triangular points). Out of the three newly obtained equilibrium points, a pair of non-collinear points are equidistantly placed above and below the $y-$axis named $L_{4,5(N)}$ and the third is lying on the $x-$axis between the largest primary and collinear equilibrium point L_1, named $L_{3\alpha}$. The shift in position of these equilibrium points with change in the perturbing forces was also studied graphically. Secondly, analytical methods were employed to obtain the equilibrium points for the model. Analytically, only six equilibrium points were obtained. Other than the points analogues to the five Lagrangian points, the existence of another collinear point $L_{3\alpha}$ was verified analytically. The graphical representation of these equilibrium points as a function of different perturbing forces, taking the other parameters as constant according to Sun-Jupiter system showed the dependence of the position of the points on various equilibrium points. And in most of the cases, the numerically obtained depiction was found to be the same as that analytically observed. Both studies showed that all the perturbing forces as well as the mass parameter effect the position of all the equilibrium points. The triangular equilibrium points $L_{4,5}$ and non-collinear points $L_{4,5(N)}$ were found to be most affected by the radiation factor q_1, then mass parameter μ and then the circumstellar belt. All the collinear points were found to be affected by mass parameter μ, oblateness parameters A_1 and A_2 and thickness of circumstellar belt h.

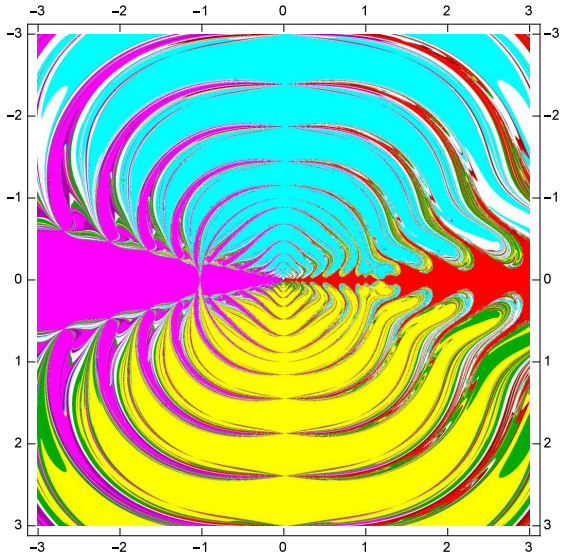

(a) Neglecting the effect of circumstellar belt

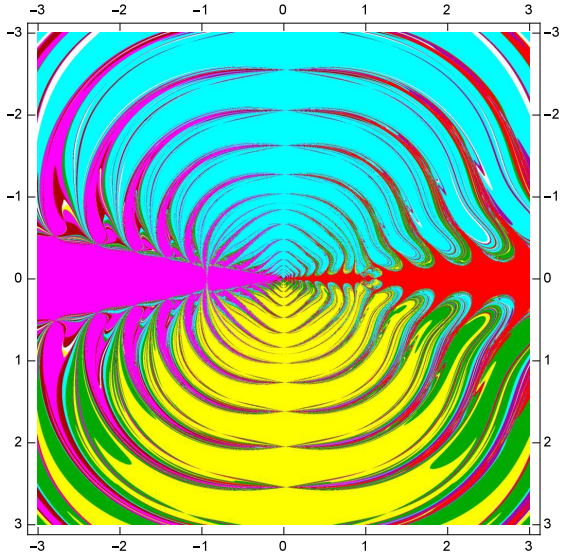

(b) With the effect of circumstellar belt

Fig. 13. Fractal basin on the $\bar{x}\bar{y}-$plane for the equilibrium points for Sun-Jupiter system

The fractal basins of convergence of these points were also studied and it was observed that the basins are affected by the mass parameter, radiation pressure as well as the circumstellar belt. However, both the structure and extent of the basins were found unaffected by oblateness parameters and eccentricity e.

References

Ammar M. K., 2008, *Ap & SS, p.*393–408*, 313*
Chakraborty A., Narayan A., Ishwar B., 2021, *FEW-BODY SYST, p.15, 62*
Chermnykh S. V., 1987, *Vestn. Leningr. Mat. Astron., p.73–77, 2*
Danby J. M. A., 1988, *William-Bell Inc., Virginia.*
Gong S., Liu C., 2016, *MNRAS, p.547–533, 462(1)*
Grebnikov E. A., 1986, *NAUKA, Moscow (Revised)*
Idrisi M. J., Ullah M. S., Kumar V., 2021, *New Astron, p.101449, 82*
Jiang I-G, Yeh L-C, 2004, *Int J Bifurcat Chaos, p. 3153-3166, 14(9)*
Jiang I.-G., Yeh L.-C., 2006, *Ap & SS, p.341-348, 305(4)*
Kalvouridis T. J., Gousidou-Koutita M. Ch., 2012, *Appl. Math., p. 541-548, 3*
Kushvah B.S., 2008, *Ap & SS, p.41–50, 318*
Kushvah B.S., 2009, *Ap & SS, p.57-63, 323*
Kushvah B.S., 2011, *Ap & SS, p.99–106, 332*
Kushvah B.S., Kishor, R. & Dolas, U., 2012,*Ap & SS, p. 115, 337*
Kishor R. & Kushvah, B. S., 2013, *MNRAS, p. 1741–1749, 436*
Liu C., Gong S., 2017, *MNRAS, p.3576–3587, 469(3)*
Mako Z., Szenkovits F., 2004, *Celest. Mech. Dyn. Astron., p.51-58,90*
Mako, Z., Szenkovits F., 2005, *PADEU, p. 21, 15.*
Papadakis K.E., 2004, *A & A, p.1133–1142, 425*
Papadakis K.E., 2005, *Ap & SS, p.67-81, 299*
Papadakis K.E.: 2005, *Ap & SS, p.129-148, 299*
Qian, Y-J., Yang, L-Y., Yang X-D, Zhang W., 2018, *Astrodynamics, p.147–159, 2(2)*
Roy A. E., Walker I. W., MacDonald, A. J. C., 1985, *In: Proceedings of the Stability of the Solar System and Its Minor Natural and Artificial Bodies, pp. 151–174. Advanced Study Institute, Cortina d'Ampezzo*
Schulz E., 2012, *The ApJ, 7p., 747 (106)*
Szebehely V., Giacaglia G. O., 1964, *Astron. J., p.230, 69*
Szebehely V., 1967, *Academic Press, Cambridge, USA*
Vinti J., Der G., Bonavito N., 1998, *American Institute of Aeronautics and Astronautics, Reston (ebook)*
Yeh L.-C., Jiang I.-G., 2006, *Ap & SS, p. 189-200, 306*